ULTRASOUND IMAGING LV TRACKING WITH ADAPTIVE WINDOW SIZE AND AUTOMATIC HYPER-PARAMETER ESTIMATION

Jacinto Nascimento[1] *and João Sanches*[1,2]

Instituto de Sistemas e Robótica[1] Instituto Superior Técnico[2]
1049-001 Lisboa,
Portugal

ABSTRACT

The segmentation of the heart's *left ventricle* (LV) chamber in several medical imaging modalities, e.g. *Ultrasound* (US) and *Magnetic Resonance* (MRI), is important from a clinical point of view in the diagnosis of certain cardiopathies. Manual segmentation is difficult, not accurate and time consuming. Therefore, automatic segmentation and tracking during cardiac cycles is needed. In this paper an automatic algorithm to segment the LV boundary along a cardiac cycle from ultrasound image sequences is used and a Bayesian despeckling algorithm is proposed. The prior parameter of the Bayesian filter is automatically estimated and an automatic window size selection strategy in used to adapt its dimension to the statistical characteristics of the image in the vicinity of the deformable contour model which segments the LV boundary. Sequences of real ultrasound images are used to illustrate the effectiveness of the approach and a comparison with other state-of-the-art filtering algorithms is provided.

***Index Terms*—** Left ventricle, total variation, tracking, ultrasound imaging.

1. INTRODUCTION

The segmentation of the heart's *left ventricle* (LV) chamber in several medical imaging modalities, e.g. *Ultrasound* (US) and *Magnetic Resonance* (MRI), is important from a clinical point of view in the diagnosis of certain cardiopathies. Manual segmentation is difficult, not accurate and time consuming and, therefore, automatic segmentation and tracking during cardiac cycles is needed.

These images present low *signal to noise ratio* (SNR) and are corrupted by a type of multiplicative noise, called *speckle* [1]. This type of noise usually appears in acquisition processes involving coherent radiation like *LASER* [2], *Ultrasound* [3] and *Synthetic Aperture Radar* (SAR) [4]. The most used paradigm *Additive White Gaussian Noise* (AWGN) is not appropriate to deal with this medical imaging modality in which the noise can not be assumed additive neither variance space invariant across the image.

Several techniques have been proposed to reduce the speckle noise without distorting the relevant clinical details, e.g. *median filtering* [5], *anisotropic diffusion* [6], *wavelet soft thresholding* [7] and others approaches, such as, adaptive window stochastic [8]. Bayesian methods has been successfully used [9] in several biological and medical imaging modalities. In the Bayesian framework used in this paper the minimizer of an energy function is the desired denoised one. This energy function is the sum of two terms: the first, called *data fidelity term*, pulls the solution toward the data; the second, is the prior term which regularizes the solution to remove the noise. The prior parameter α allows to tune the degree of smoothness of the solution. Large values of α makes it possible to remove large amounts of noise but also some anatomical details needed for the diagnosis. Small values of α allows to keep these details but also keeps the noise. Therefore, a tradeoff must be attained.

In this paper a Bayesian algorithm for *despeckle* ultrasound images is proposed where the prior parameter and the region of support of the kernel are automatically selected based on the statistical properties of the image in the vicinity of the active contour. The proposed algorithm is termed as TV-AWS (*Total Variation with Automatic Window Size*).

The TV-AWS method is compared with an unifying denoising framework, proposed in [10], and with a state-of-the-art SBF method [8] using real ultrasound sequences.

This work was partially supported by FCT, Portuguese Ministry of Science an Technology and Higher Education (which includes FEDER funds).

2. PROBLEM FORMULATION

Let $\mathbf{X}$ be a $N \times M$ unknown image to be estimated from the noisy image $\mathbf{Y}$. The estimation of X, formulated in a Bayesian framework, is obtained by solving the following optimization problem

$$\hat{\mathbf{X}} = \arg\min_{\mathbf{X}} E(\mathbf{X}, \mathbf{Y}) \tag{1}$$

Using the *maximum a posteriori* (MAP) criterion the energy function is

$$\begin{aligned} E(\mathbf{Y}, \mathbf{X}) &= -\log\left[p(\mathbf{Y}|\mathbf{X})p(\mathbf{X}, \alpha)\right] \\ &= \underbrace{-\log\left[p(\mathbf{Y}|\mathbf{X})\right]}_{E_Y(\mathbf{Y},\mathbf{X})} \underbrace{-\log\left[p(\mathbf{X}, \alpha)\right]}_{E_X(\mathbf{X})} \end{aligned} \tag{2}$$

where $p(\mathbf{Y}|\mathbf{X})$ is the *likelihood function*, $p(\mathbf{X}, \alpha)$ is a prior distribution and α is a parameter; $E_Y(\mathbf{X}, \mathbf{Y})$, called *data fidelity term*, depends on the observation model and attracts the solution toward the data, and $E_X(\mathbf{X})$, called *prior term* or *internal energy*, regularizes the solution, removes the noise and incorporates a priori knowledge about the solution. In this paper the *speckle* noise that corrupts the ultrasound images is modeled by a Rayleigh distribution, i.e. $p(y|x) = (y/x)e^{-y^2/2x}$, and it is assumed that the observations are independent, i.e. $p(\mathbf{Y}|\mathbf{X}) = \prod_{i,j=1}^{N,M} p(y(i,j)|x(i,j))$. This leads to

$$E_Y(\mathbf{Y}, \mathbf{X}) = \sum_{i,j=1}^{N,M} \frac{y(i,j)}{x(i,j)} e^{-\frac{y^2(i,j)}{2x^2(i,j)}} \tag{3}$$

where $\mathbf{X}$ is assumed to be a band-limited signal described by a *Markov Random Field* (MRF) defined using neighborhood interactions among set of pixels. The prior distribution, under these assumptions, is a Gibbs distribution, i.e. $P(\mathbf{X}) = Z^{-1}e^{-U(\mathbf{X})}$ where Z is the partition function and $U(\mathbf{X})$ is the so called *Gibbs energy*.

The Gibbs energy, $U(\mathbf{X})$ smooths the solution and reduces the noise. However, it must be carefully designed in order to not distort the transitions containing relevant anatomic details. To preserve these details several authors have proposed Gibbs distributions that preserve transitions, called *edge preserving priors*. One of the most used is based on the *total variation* (TV) where the Gibbs energy is defined as follows

$$U(\mathbf{X}) = \sum_{i,j=1}^{N,M} g(i,j) \tag{4}$$

where $g(i,j)$ is the gradient magnitude computed at the pixel (i,j) which may be computed by

$$g(i,j) = \sqrt{(x(i,j) - x(i-1,j))^2 + (x(i,j) - x(i,j-1))^2)} \tag{5}$$

The energy to be minimized is therefore

$$E(\mathbf{Y},\mathbf{X}) = \sum_{i,j=1}^{N,M} \left[\frac{y(i,j)}{x(i,j)} e^{-\frac{y^2(i,j)}{2x^2(i,j)}} + \alpha g(i,j) \right] \tag{6}$$

The prior parameter α is used to control the smoothing effect in the final solution by tuning the interaction strength among neighboring nodes. The larger is α the smoother is the final solution. The selection of α is a difficult and open problem. Most of the time this parameter is chosen manually in a trial and error basis but several authors already have proposed methods to select it automatically [11]. In this paper a new automatic method is proposed.

Let us factorize the prior distribution

$$p(\mathbf{X}) = \frac{1}{Z} e^{-\alpha TV} = \prod_{i,j=1}^{N,M} \frac{1}{z(i,j)} e^{-\alpha g(i,j)} \tag{7}$$

which may be viewed as the joint probability density function of NM *independent and identically distributed* (i.i.d) random variables with probability $p(g(i,j)) = \frac{1}{z(i,j)} e^{-\alpha g(i,j)}$. The independence assumption of the gradients may be not realistic. However, is a straightforward algebraic consequence of the Gibbs distribution that describes $\mathbf{X}$. Furthermore, this assumption leads to consistent results, validating the above assumption. This distribution is a true probability density function if $\int_0^\infty p(g)dg = 1$ where the integration is performed only for R^+ because $g(i,j) \geq 0$. From equation (2) it is derived the following result: $z(i,j) = 1/\alpha$, which means that $p(\mathbf{X}) = \alpha^{NM} e^{-\alpha TV(\mathbf{X})}$. The energy function to be minimized is therefore

$$E(\mathbf{Y},\mathbf{X},\alpha) = E_Y(\mathbf{Y},\mathbf{X}) + \alpha TV(\mathbf{X}) - NM\log(\alpha) \tag{8}$$

The optimum value for α is the minimizer of $E(\mathbf{Y},\mathbf{X},\alpha)$

$$\alpha_{opt} = \arg\min_{\alpha} E(\mathbf{Y},\mathbf{X},\alpha) \tag{9}$$

which may be computed by solving the following equation $\frac{\partial E(\mathbf{Y},\mathbf{X},\alpha)}{\partial \alpha} = TV(\mathbf{X}) - \frac{NM}{\alpha} = 0$, leading to

$$\alpha_{opt} = \frac{NM}{TV} = \frac{1}{\bar{g}} \tag{10}$$

where $\bar{g}$ is the average value of the gradient magnitude computed over all pixels of the image.

The results obtained with this optimum parameter, α_{opt} are usually over smoothed. In fact, the mean of the gradient magnitude across the whole image tends to decrease due the homogeneous regions which leads to an increase on the parameter $\alpha_{opt} = 1/\bar{g}$. To avoid this effect, instead of using a constant optimum prior parameter computed with all image pixels, we propose to use an adaptive scheme where the prior parameter is adjusted to the local characteristics of the image, that is

$$\alpha(i,j)_{opt} = (\mathbf{G} * \mathbf{H})(i,j) \tag{11}$$

where $\mathbf{G}$ is a $N \times M$ matrix containing the gradient magnitude at each pixel and $\mathbf{H}$ is a $n \times m$ convolution mask. For instance, if $\mathbf{H}$ is a rectangular window each $\alpha(i,j)_{opt}$ is the average value of the gradient magnitude computed around the $(i,j)^{th}$ pixel.

Here, the *flattop* window implemented in Matlab is used because comparative experimental results have shown that leads to the better results.

The energy function

$$E(\mathbf{Y},\mathbf{X}) = \sum_{i,j=1}^{N,M} \left[\frac{y(i,j)}{x(i,j)} e^{-\frac{y^2(i,j)}{2x^2(i,j)}} + \frac{g(i,j)}{(\mathbf{G} * \mathbf{H})(i,j)} \right] \tag{12}$$

is minimized by using a *Majorize/Minimize* (MM) optimization strategy, formulated as a *Sylvester/Lyapunov* equation for which there are fast and efficient algorithms described in the literature and the fixed point method as described in [12]. This leads to

$$\mathbf{\Phi}_N \mathbf{X} + \mathbf{X}\mathbf{\Phi}_M + \mathbf{C}(\mathbf{X}_{t-1}) = 0 \tag{13}$$

where $\mathbf{\Phi}_N = \frac{\beta}{2}\mathbf{I}_N + \mathbf{\Theta}_N$; $\mathbf{\Phi}_M = \frac{\beta}{2}\mathbf{I}_M + \mathbf{\Theta}_M$ and $\mathbf{C}(\mathbf{X}_{t-1}) = \mathbf{G}_{t-1} \odot \tilde{G} \odot \frac{(\mathbf{X}_{t-1} - (1/2)\mathbf{Y}^{\odot 2})}{2\mathbf{X}_{t-1}^{\odot 2}} - \beta \mathbf{X}_{t-1}$. The matrices $\mathbf{I}_N, \mathbf{I}_M$ are N and M dimensional identity matrices respectively; $\tilde{G} = \mathbf{G}_{t-1} * \mathbf{H}$ and β is a conditioner parameter, important to stabilize the iterative algorithm but does not change the final solution, only the convergence properties; $\odot$ denotes an element wise operation and t the estimation at t^{th}iteration. The matrix $\mathbf{\Theta}$ is defined in [12].

3. SIZE WINDOW ESTIMATION

This section describes the procedure to automatically select the $\mathbf{H}$ window size. The criterion used herein is inspired by [8] which is based on the fact that the ratio of the mean to standard deviation of a Rayleigh distribution is constant, $R = \sqrt{\frac{\pi}{4-\pi}} \approx 1.9$. However the real ultrasound images do not precisely follow a true Rayleigh distribution. Thus, the adopted strategy is to select the size of the window which distribution is as similar as possible with the Rayleigh one.

At each pixel of the US image, we dynamically choose the window of dimension $\hat{L} \times \hat{L}$ so that

$$\hat{L} = \arg\min_{L \in \mathcal{S}} |R - R_{L \times L}| \tag{14}$$

where $R_{L \times L}$ is the ratio of the mean to standard deviation within a neighborhood window size L. We allowed for a square window with odd row and column to vary in $\mathcal{S} = \{3, 5, \ldots, 21\}$ at each pixel.

This method allows us to select the best size window for each pixel. Fig. 1(a) shows an US image of the LV, Fig. 1(b) shows the corresponding *"window size image"*, where the intensity of each pixel is the window size to be applied at that pixel. It is possible to see the LV contour in a darker region (see Fig. 1(b)). Darker regions correspond to smaller window sizes, brighter regions correspond to larger windows. This means that at the discontinuities, the window should be small, whereas in homogeneous regions the window should be larger. Since the goal of this paper is to track the boundary of the LV, we conclude that smaller sizes for the window are desirable.

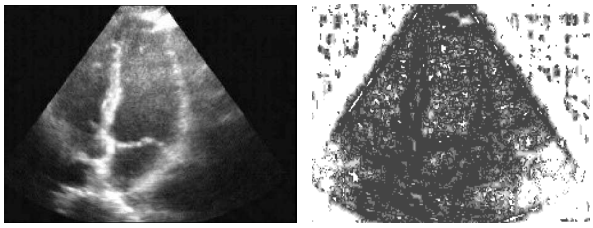

(a) (b)

Fig. 1. (a) Ultrasound image of the LV; (b) *window size image*.

The selection of the window size to be applied throughout the sequences is related with the initialization of the tracking process. This makes the procedure fully automatic. The initialization of the S-PDAF (*Shape Probabilistic Data Association*) tracker [13] requires that, the user must provide a set of points of the curve (samples of the active contour) located at the LV contour in the first frame (see dots in Fig. 2(a)). Then, orthogonal lines radiating from these points are automatically constructed giving the *validation gate* (region in which the features are detected from the image; we refer the reader to [13]). Then, we compute the intensity profiles of all orthogonal lines in the *window size image*. Fig.2 (c) shows one orthogonal line, and Fig.2 (d) shows the corresponding intensity profile. After this stage, we compute the histogram of the mean intensity profiles of all orthogonal lines. The result is shown in Fig. 2 (b), which justifies the window size of 3 pixel used in the evaluation presented in the Section 4.

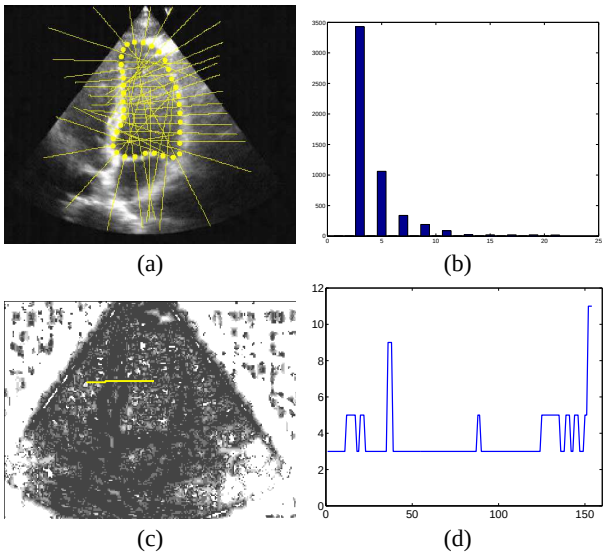

(a) (b)

(c) (d)

Fig. 2. (a) Ultrasound image of the LV with the contour initialization (dots), and the validation gate (orthogonal lines); (b) histogram of the window sizes estimated from the validation gate; (c) *window size image* with one orthogonal line and (d) the corresponding intensity profile taken at that orthogonal line.

4. EXPERIMENTAL RESULTS

In this section we present an example of application concerning the tracking of the left ventricle (LV). Two sequences of the ultrasound LV are used. These sequences correspond to real medical exams performed in two different people. The sequences were obtained at a frame rate of 15 frames sec^{-1} using an ultrasound probe operating at 1.7 Mhz. The size of the ultrasound sequences are: (i) case ♯1: 490 frames (26 cycles); (ii) case ♯2: 470 frames (19 cycles). The tracker used in this study is the S-PDAF. Details about this method can be found in [13]. In this study we provide a comparison of the following denoising methods: i) median filtering; ii) L_2 prior; iii) TV prior; iv) Benford prior and v) proposed method; vi) SBF [8]. The methods ii) to v) are implemented in the denoising unified framework proposed in [10].

The ultrasound sequences were first pre-processed by each of the six denoising algorithms mentioned above. In this way, we obtain a total of 12 pre-processed sequences (six for each case). Then, we run the tracker for each of the 12 pre-processed sequences, obtaining 12 sets of estimated contours of the LV.

Objective Evaluation

To evaluate the performance of the algorithms we compare the contour estimates provided by the tracker with the ground truth (reference contours) provided by a cardiologist of Hospital Amadora-Sintra. This comparison is done as follows: we selected four images from each cardiac cycle (two images in the systole phase and two images in the diastole phase) and asked to a doctor to manually define the LV contour for each of these images. The specialist segmented 80 images: 40 images from each sequence, 20 of them extracted during the systole phase and other 20 images during the diastole phase. The selection of the frames was random.

Five metrics were used in these tests: i) Hausdorff distance (*cf.* [14]); ii) the average distance; iii) Hammoude distance (*cf.* [15]); iv) Mean Sum of Squared Distance (MSSD) (*cf.* [16]) and Mean Absolute Distance (MAD) (*cf.* [17]). Next, we briefly describe them.

Let $\mathcal{X} = \{\mathbf{x}_1, \mathbf{x}_2, \ldots, \mathbf{x}_{N_x}\}$, and $\mathcal{Y} = \{\mathbf{y}_1, \mathbf{y}_2, \ldots, \mathbf{y}_{N_y}\}$, be two sets of points obtained by sampling the estimated contour and the reference contour. The smallest distance from a point $\mathbf{x}_i$ to the curve $\mathcal{Y}$ is

$$d(\mathbf{x}_i, \mathcal{Y}) = \min_j ||\mathbf{y}_j - \mathbf{x}_i|| \tag{15}$$

This is known as the distance to the closest point (DCP). The average distance between the sets $\mathcal{X}$, $\mathcal{Y}$ is

$$d_{AV} = \frac{1}{N_x} \sum_{i=1}^{N_x} d(\mathbf{x}_i, \mathcal{Y}) \tag{16}$$

where N_x is the length of the $\mathcal{X}$ The Hausdorff distance between both sets is defined as the maximum of the DCP's between the two curves

$$d_{HDF}(\mathcal{X}, \mathcal{Y}) = \max \left[\max_i \{d(\mathbf{x}_i, \mathcal{Y})\}, \max_j \{d(\mathbf{y}_j, \mathcal{X})\} \right] \tag{17}$$

For Hammoude distance let us define $R_\mathcal{X}$, $R_\mathcal{Y}$ as the image regions inside the two contours. We compute the number of points which belongs to only one of these regions and normalize it by the number of points of the union of both regions

$$d_{HMD} = \frac{\sharp\ (R_\mathcal{X} \cup R_\mathcal{Y}) - (R_\mathcal{X} \cap R_\mathcal{Y})}{\sharp (R_\mathcal{X} \cup R_\mathcal{Y})} \tag{18}$$

If we represent the regions $R_\mathcal{X}$, $R_\mathcal{Y}$ by two binary images, the d_{HMD} is equal to the Hamming distance between the binary images, normalized by the area of their sum. The Hammoude distance is a normalized version of the Hamming distance which is widely used to compare binary strings and images in information theory.

The MSSD and MAD distances are defined as follows

$$d_{MSSD}(\mathcal{X}, \mathcal{Y}) = \left\{ \frac{1}{n} \sum_{i=1}^{n} d^2(\mathbf{x}_i, \mathcal{Y}) + \frac{1}{m} \sum_{i=1}^{m} d^2(\mathbf{y}_i, \mathcal{X}) \right\} \tag{19}$$

Table 1. Metrics mean values for the first and second sequences.

		Median	L_2	TV	Bfd	$TV-AWS$	SBF
d_{Hmd}	sequence #1	0.20	0.18	0.19	0.17	**0.14**	0.18
	sequence #2	0.25	0.22	0.19	0.20	**0.18**	**0.18**
d_{Av}	sequence #1	4.66	4.20	4.19	3.81	**3.30**	4.32
	sequence #2	4.57	4.33	**3.57**	3.74	3.68	3.75
d_{Hdf}	sequence #1	13.74	12.83	12.78	11.33	**9.70**	13.25
	sequence #2	12.17	11.16	**9.48**	9.95	9.95	9.86
d_{MSSD}	sequence #1	2.13	1.61	1.57	1.26	**0.96**	1.62
	sequence #2	2.14	1.55	1.46	1.79	1.31	**1.19**
d_{MAD}	sequence #1	0.25	0.23	0.23	0.21	**0.19**	0.24
	sequence #2	0.26	0.24	**0.20**	0.21	**0.20**	**0.20**

$$d_{MAD}(\mathcal{X},\mathcal{Y}) = \Big\{\frac{1}{n}\sum_{i=1}^{n} d(\mathbf{x}_i,\mathcal{Y}) + \frac{1}{m}\sum_{i=1}^{m} d(\mathbf{y}_i,\mathcal{X})\Big\} \qquad (20)$$

where d is the DCP given as in (15). In the two above distances, they do not give higher weights to longer sequences. In this paper, the distances in (19) and (20) do not have point correspondence as originally proposed in [16,17]. Thus, the nearest point from the other contour is taking as the corresponding point.

Table 1 shows the fidelity in the representation of the LV contour obtained in the two US sequences, which is an important feature when tracking the contour of the object of interest. These values correspond to the mean values of the metrics described above. From Table 1 we conclude that, in the first sequence, the proposed approach exhibits the best results. In the second sequence, the best scores are shared with the proposed method the TV prior as well as the state-of-the-art SBF method. We can say that the proposed approach provides competitive results which are capable to compete with other methods recently proposed.

5. CONCLUSIONS

This paper proposes a new denoising algorithm with automatic window size and hyper parameter estimation. A comparison between the proposed approach and an unified framework [10] as well as a state-of the art algorithm SBF [8] is provided. The experimental results testify that the method proposed herein is capable to provide competitive results.

Although remarkable results are achieved, further work will address spatial-temporal concerns. In fact, we have used the same window size for all points along the LV contour during all frames in the sequence. We believe that it is possible to improve the results, providing higher accuracy estimates of the LV contour, if the hyper parameter estimation is performed in a spatiotemporal vary window.

6. ACKNOWLEDGEMENT

The authors would like to thank Peter C. Tay, Scott T. Acton and John A. Hossack for providing the source code of the SBF method proposed in [8]. They would also like to thank Dr. A. Freitas from the Hospital Amadora-Sintra for providing the ground truth segmentation of the left ventricle.

7. REFERENCES

[1] Abbot J. and Thurstone F., "Acoustic speckle: Theory and experimental analysis," *Ultrasound Imaging*, vol. 1, pp. 303–324, 1979.

[2] B. Zagar and H. Weiss, "Processing of laser speckle interferometer signals for high precision strain measurement," in *Proc. of the 8th International Symposium on Artificial Intelligence Based Measurement and Control*, 1991, vol. 1, pp. 99–105.

[3] C. Burckhardt, "Speckle in ultrasound b-mode scans," *IEEE Transactions on Sonics and Ultrsonics*, vol. SU-25, no. 1, pp. 1–6, Jan. 1978.

[4] Peiliang Xu, "Despeckling sar-type multiplicative noise," *International Journal of Remote Sensing*, vol. 20, no. 13, pp. 2577– 596, Sep. 1999.

[5] T. Loupas, W. McDicken, and P. Allan, "An adaptive weighted median filter for speckle suppression in medical ultrasonic images," *IEEE Transactions on Circuits and Systems*, vol. 36, pp. 129–135, Jan. 1989.

[6] Karl Krissian, Kirby Vosburgh, Ron Kikinis, and Carl-Fredrik Westin, "Speckle-constrained anisotropic diffusion for ultrasound images," in *Proceedings of IEEE Computer Society Conference on Computer Vision and Pattern Recognition ('05)*, San Diego CA, USA, June 2005, pp. 547 – 552.

[7] S. Gupta, L. Kaur, R. C. Chauhan, and S. C. Saxena, "A wavelet based statistical approach for speckle reduction in medical ultrasound images," *Medical and Biological Engineering and computing*, vol. 42, 2004.

[8] Peter C. Tay, Scott T. Acton, and John A. Hossack, "Ultrasound despeckling using an adapatative window steochastic approach.," in *Proc. of the Int. Conf. on Image Processing (ICIP 2006)*, Atlanta, GA, USA, April 2006, pp. 2549–2552.

[9] Z. Zeng and I. Cumming, "Bayesian speckle noise reduction using the discrete wavelet transform," in *International geoscience and remote sensing symposium*, July 1998, pp. 6–10.

[10] J. Sanches, J. Nascimento, and J. Marques, "An unified framework for bayesian denoising for several medical and biological imaging modalities," in *Proc. of the Int. Conf. of the IEEE Eng. Medicine and Biology Society*, 2007.

[11] Peter R. Johnston and Ramesh M. Gulrajani, "Selecting the corner in the -curve approach to tikhonov regularization," *IEEE TRANSACTIONS ON BIOMEDICAL ENGINEERING*, vol. 47, no. 9, pp. 1293–1296, September 2000.

[12] Nascimento J., Sanches J.M., and Marques J.S., "An unified framework for bayesian denoising for several medical and biological imaging modalities," in *Proc. of the IEEE EMBC 2007*, Lyon, France, August 23-26 2007.

[13] J. Nascimento and J. S. Marques, "Robust shape tracking in the presence of cluttered background," *IEEE Trans. Multimedia*, vol. 6, no. 6, pp. 852–861, December 2004.

[14] D. P. Huttenlocher, G. A. Klanderman, and W. J. Rucklidge, "Comparing images using Hausdorff distance," *IEEE Trans. Pattern Anal. Machine Intell.*, vol. 15, pp. 850–863, 1993.

[15] A. Hammoude, *Computer-assited endocardial border identification from a sequence of two-dimensional echocardiographic images*, Ph.D. thesis, Univ. Washington, Seattle, WA, 1988.

[16] Y. Akgul and C. Kambhamettu, "A coarse-to-fine deformable contour optimization framework," *IEEE Trans. Pattern Anal. Machine Intell.*, vol. 25, no. 2, pp. 174–186, 2003.

[17] I. Mikić, S. Krucinki, and J. D. Thomas, "Segmentation and tracking in echocardiographic sequences: Active contours guided by optical flow estimates," *IEEE Trans. Med. Imag.*, vol. 17, no. 2, pp. 274–284, 1998.